

Irregular Aharonov–Bohm oscillations in loops with a finite aspect ratio

K. N. Pichugin and A. F. Sadreev

*L. V. Kirenskii Institute of Physics, Siberian Division of Russian Academy of Sciences,
660036 Krasnoyarsk, Russia*

(Submitted 28 April 1995)

Zh. Éksp. Teor. Fiz. **109**, 546–561 (February 1996)

The paper describes transport properties of a mesoscopic loop with a finite aspect ratio with two terminals in a magnetic field. The loop is rectangular and is characterized by a ratio d/L , where L is the loop dimension, and d is the width of its segments. If the loop is fairly narrow ($d/L=1/9$), the curve of its conductance versus magnetic flux can be divided into three regions. In its first region, where the magnetic length satisfies $l_H=\sqrt{\hbar c/eB}\geq 1.3d$, the Aharonov–Bohm (AB) oscillations are regular and quasiperiodic. The current density also oscillates and forms a laminar pattern except regions next to the terminals, where one vortex or a vortex–antivortex pair is formed. The second region is characterized by the inequality $d\leq l_H\leq 1.3d$ and is strongly affected by quantum oscillations which lead to irregular AB oscillations. In the third region ($l_H\leq d$) electron transport across the loop is totally blocked and electrons are confined in the input terminal. In the case of multichannel transport (the paper considers only one and two-channel cases) AB oscillations are irregular, and the electron current density forms a convection vortex pattern. At a higher ratio $d/L=1/4$ the range of irregular AB oscillations is wider. © 1996 American Institute of Physics. [S1063-7761(96)01602-1]

1. INTRODUCTION

The intense interest in transport properties of mesoscopic and nanostructures shaped as quantum wires, dots, heterostructures, etc., is driven by the progress in nanotechnology using molecular-beam epitaxy and lithography.¹ Structures fabricated by these techniques are of such high quality that their transport properties are controlled by the coherence of electron wave functions across them. Aharonov–Bohm (AB) oscillations² in metal (Au, Ag, and Cu) and semiconductor (based on GaAs) loops^{3–5} and the quantum Hall effect^{6,7} are spectacular manifestations of the electron coherence in these structures.

AB oscillations arise because an electron conducted from the input terminal into a loop acquires an additional phase

$$\frac{\delta}{2} = \pm \frac{e}{\hbar c} \int d\mathbf{r} \cdot \mathbf{A},$$

where the sign of the integral depends on which branch of the loop contains the electron trajectory. As a result, the total phase shift at the output terminal is

$$\frac{\pi e H_0 r^2}{\hbar c} = \frac{2\pi\Phi}{\Phi_0} = 2\pi\gamma, \quad (1)$$

where H_0 is the external magnetic field perpendicular to the loop plane, Φ is the magnetic flux through the ring, and Φ_0 is the magnetic-flux quantum. This equation indicates that the electron transport should be periodic in the reduced flux γ with a period equal to unity.

The simplest approach to AB oscillations is to consider a two-terminal structure consisting of one loop and two electrodes connected to it. If the electron motion across such a structure is one-dimensional and coherent, oscillations of its

conductance will be strictly periodic with a period equal to unity. But if the electron coherence length in the loop is comparable to or smaller than its dimension, the shape of the AB oscillations may alter owing to interference with trajectories of electrons backscattered from impurities, and the period of AB oscillations in contaminated cylindrical structures may be $1/2$.^{8,9} Several authors^{10–12} attempted to find an exact solution of the quantum-mechanical problem of the electron transport across a mesoscopic one-dimensional, two-terminal loop with two arbitrary scatterers. The period of the oscillations in this solution was unity, although curves of the transmission probability versus magnetic flux clearly demonstrate the presence of higher harmonics. The parameters of scatterers for which the second harmonic was dominant, i.e., the period of oscillations was $1/2$, were also determined.¹¹ A similar effect is caused by inelastic scattering from dynamic scatterers like phonons.¹³ To end our brief review of one-dimensional rings, we should note the importance of averaging over scatterers.^{14,15} After this procedure the unit period is eliminated in the thermodynamic limit, and only the period $1/2$ is observed. A calculation of AB oscillations in mesoscopic rings with ring segments modelled as N -channel conductors demonstrated that oscillations with the unit and one-half periods fall with N as $1/N$ when the conductance is averaged over the channels.¹⁶

In real experiments regular AB oscillations are not observed in loops with dimensions of 100–500 nm and a segment width $d=40$ nm. Fourier transforms of AB oscillations^{5,17} indicate that they contain a harmonic with the unit period and an additional harmonic with the period $1/2$. Besides, Fourier transforms of AB oscillations show a considerable contribution from aperiodic fluctuations. The contribution from aperiodic fluctuations increases as a function of the ratio d/L , a one-third harmonic emerges, and the

widths of periodic peaks plotted against the magnetic field, including those with the unit period, also increase. Stone¹⁸ was the first to calculate numerically these quantum fluctuations in a two-dimensional strip in a magnetic field using the quantum jump model with random energies of the scatterers. He demonstrated the existence of reproducible fluctuations in electron transport due to the microscopic configuration of the sample. These fluctuations are considerably stronger if quantum states are localized. As for the quantum Hall effect, a similar suggestion that localized electron states may bring about intense quantum fluctuations of the low-temperature conductance was made by Jain and Kivelson.^{19,20} In particular, a strip electron waveguide with an internal barrier was considered, and large fluctuations in the transmission of electrons tunnelling via localized states were detected. Note also the work by Shapiro,²¹ who found that in a planar waveguide corrections to the quantum Hall effect are on the order of $(d/l_H)^2$, where

$$l_H = \sqrt{\frac{\hbar c}{eH_0}} \quad (2)$$

is the magnetic length. Experimental studies of the quantum Hall effect in multiterminal mesoscopic loops²² demonstrated that, first, only those theories in which no averaging over impurities is used are applicable and, second, at low magnetic fields aperiodic AB oscillations are due to the quantum AB interference of electrons scattered from impurities or geometrical irregularities of their trajectories.

Concluding our review of two-dimensional electron waveguides under magnetic field, let us consider several works in which microscopic current distributions were calculated, as a rule, numerically. A detailed analysis of current distributions in two-dimensional straight waveguides with scatterers^{23–25} or with a potential barrier,²⁶ and in curved waveguides without scatterers^{27–29} revealed fundamentally new features of the two-dimensional electron transport, which showed the quantum Hall effect from another viewpoint. The first feature is the formation of boundary states near edges of two-dimensional structures along which current flows. These states give the structure a high conductance, despite the presence of scatterers in it. The second and most interesting feature is the formation of vortex states in the electron current distribution. They may have a considerable effect on the electron transport. In systems with scatterers, states with an orbital momentum localized on impurities in a magnetic field are formed concurrently. The most impressive effect of vortices on the conductance was demon-

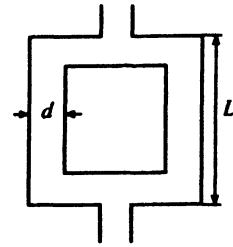


FIG. 1. Configuration of the mesoscopic loop with two terminals.

strated by Berggren and Zhen-Li Ji,²⁹ who discovered a transition from laminar to convective transport in a curved waveguide with two bends. Such transitions are accompanied by jumps in the conductance.

In this work we have numerically calculated AB oscillations in the conductance, detailed structure of wave functions and current distribution in two-dimensional loops with two wide terminals. The magnetic field is perpendicular to the loop plane. To the best of our knowledge, these characteristics of two-dimensional loops have not been calculated previously. According to Stone¹⁸ inside and outside electron trajectories in the loop enclose different magnetic fluxes, which leads to aperiodic AB oscillations. But he assumed that the electron transport in the loop was laminar. In this paper we demonstrate that even with a very small magnetic flux, $\gamma \ll 1$, the transport is not laminar because a vortex is formed in the input terminal. This makes phase shifts of electrons traveling along different trajectories equal, and AB oscillations are periodic until the magnetic length is equal to fd , where d is the width of a bend in the loop and f is the number of electron transport channels. At a higher magnetic flux, AB oscillations are irregular owing to the restructuring of wave functions inside the loop and resulting fluctuations of local current distributions in space. Finally, when the magnetic length is smaller than the aspect ratio, the electron state in the input terminal is totally localized, and the electron current across the loop is blocked. Besides, AB oscillations in the loop essentially depend on whether the electron transport is single-channel (only the fundamental mode is fed into the loop) or multichannel (several modes are fed). In the latter case AB oscillations are practically random and the current distribution is a convectional pattern of vortex chains.

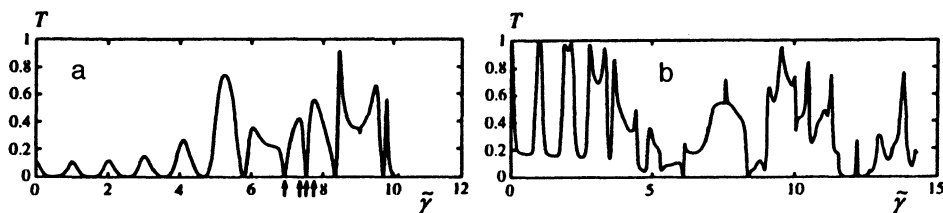


FIG. 2. Aharonov–Bohm oscillations of the probability of transmission across a narrow two-dimensional loop with a bend of width $d=12$ and an external loop dimension $L=108$; $\tilde{\gamma}$ is defined by Eq. (12) and equals the magnetic flux across the middle trajectory in the loop divided by the flux quantum: a) dimensionless energy $\epsilon=20$ (single-channel transport); b) $\epsilon=50$ (two-channel transport). The arrows indicate $\tilde{\gamma}$ corresponding to the patterns of the wave function and current shown in the following graphs.

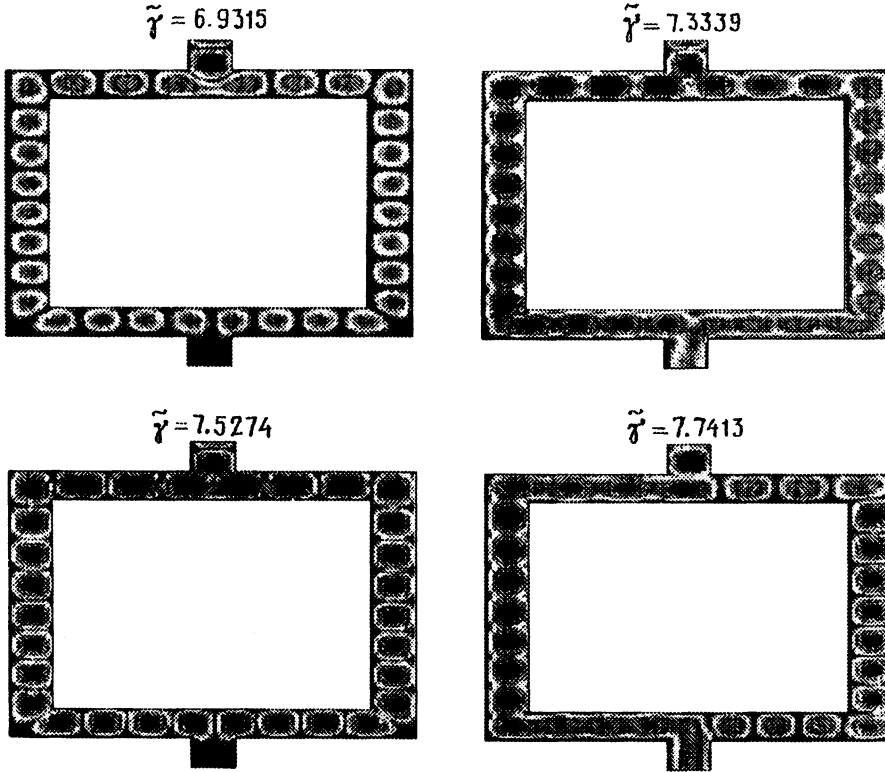


FIG. 3. Patterns of the wave function $|\psi(x,y)|$ corresponding to $\tilde{\gamma}$ indicated by arrows in Fig. 2a at $\epsilon=20$ (single-channel transport).

2. STARTING EQUATIONS

The Schrödinger equation for the stationary electron transport in a two-dimensional structure in magnetic field is

$$\left[\frac{1}{2m} \left(\mathbf{p} - \frac{e}{c} \mathbf{A} \right)^2 + V(\mathbf{x}) \right] \psi(\mathbf{x}) = E \psi(\mathbf{x}), \quad (3)$$

where \mathbf{A} is the vector potential in the Landau gauge:

$$\mathbf{A} = (-H_0 y, 0, 0), \quad (4)$$

and $V(\mathbf{x})$ is the potential confining electrons in the structure. The structure shown in Fig. 1 has the shape of a rectangular loop with two wide terminals. The Fermi energy (or chemical potential in a semiconductor structure) is uniform throughout the structure, including the terminals. The electron motion across the structure is ballistic, i.e., the coherence length is much larger than the loop dimension, which determines the upper limit on this dimension of the order of 100 nm. The magnetic field is uniform.

Equation (3) in dimensionless form is

$$\left[\left(i \frac{\partial}{\partial x} + \gamma y \right)^2 - \frac{\partial^2}{\partial y^2} \right] \psi = \epsilon \psi, \quad (5)$$

where the coordinates are divided by the loop width d ,

$$\gamma = H_0 d^2 / \Phi_0, \quad \epsilon = 2m d^2 E / \hbar^2. \quad (6)$$

Techniques for calculating the probability of transfer through a multidimensional structure, from which the conductance is derived in the Buttiker–Landauer model,^{30,31} are well developed, and this probability can be derived by several methods. The first method is to calculate directly the transfer probability using the T-matrix;^{32–34} in the second method Eq. (5) is solved numerically by finite-differences;

and in the third method the structure is separated into regions and the solution in each region is expressed as a series of its eigenfunctions, and these are matched on the boundaries. The latter technique yields good results for zero magnetic field because in this case the solutions are plane waves. This method was applied to curved waveguides^{29,35,36} and multi-terminal structures.^{37–39} But in the presence of a magnetic field the eigensolutions are parabolic cylinder functions, which makes calculations more difficult. Note also the Green's function method.^{40,41} Our approach combines several techniques. In the terminals we represent the solution as a superposition of waves, and in the loop we use numerical techniques.

Let us write the solution in the input terminal as

$$\psi_{\text{in}}(x,y) = e^{-i\kappa y} \phi_1(y) + \sum_f a_f e^{i\kappa_f y} \phi_f(y), \quad (7)$$

where the transverse functions ϕ_f are the eigenfunctions of a one-dimensional problem,

$$\left[(\kappa_f + \gamma y)^2 - \frac{\partial^2}{\partial y^2} \right] \phi_f(y) = \lambda_f \phi_f(y), \quad (8)$$

$$\epsilon = \kappa_f^2 + \lambda_f. \quad (9)$$

The axial wave numbers κ and κ_f are also made dimensionless by dividing by the terminal width d , which is equal to that of the bend in the loop. In the output terminal the solution is written as

$$\psi_{\text{out}}(x,y) = \sum_f b_f e^{i\kappa_f y} \phi_f(y). \quad (10)$$

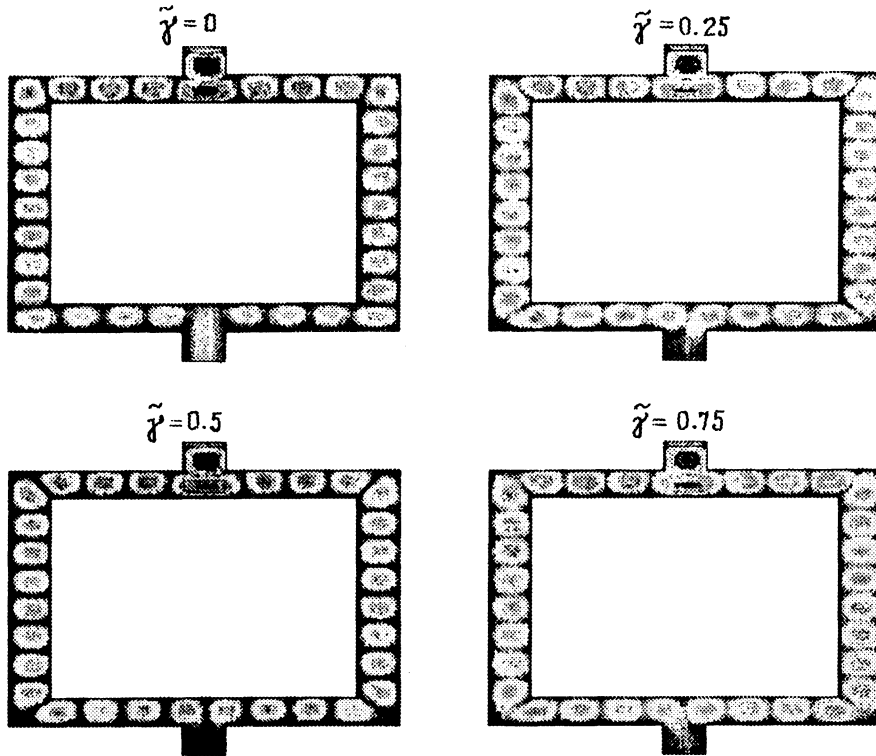


FIG. 4. Patterns similar to those in Fig. 3 in the range of small magnetic fluxes.

The finite difference equation for the functions in the loop is

$$[4 + \gamma^2 n^2 - \epsilon] \psi_{m,n} - (1 + i\gamma n) \psi_{m+1,n} - (1 - i\gamma n) \psi_{m-1,n} - \psi_{m,n+1} - \psi_{m,n-1} = 0, \quad (11)$$

where m and n run through integers from 1 to N . We construct the numerical solution starting from the upper edge of the loop, where $\psi(m,0) = \psi_{\text{in}}(x_m,0)$ or $\psi(m,0) = 0$, and ending on its lower edge, where $\psi(m,N+1) = \psi_{\text{out}}(x_m,L)$ or

$\psi(m,N+1) = 0$. As a result, we have a system of equations for the factors a_f and b_f which determine the probabilities of electron transmission and reflection through the equations

$$T = \sum_{f=1} \frac{\kappa_f}{\kappa} |b_f|^2, \quad R = \sum_{f=1} \frac{\kappa_f}{\kappa} |a_f|^2.$$

The calculation accuracy was checked by the condition $T + R = 1$, which was satisfied to within 10^{-8} .

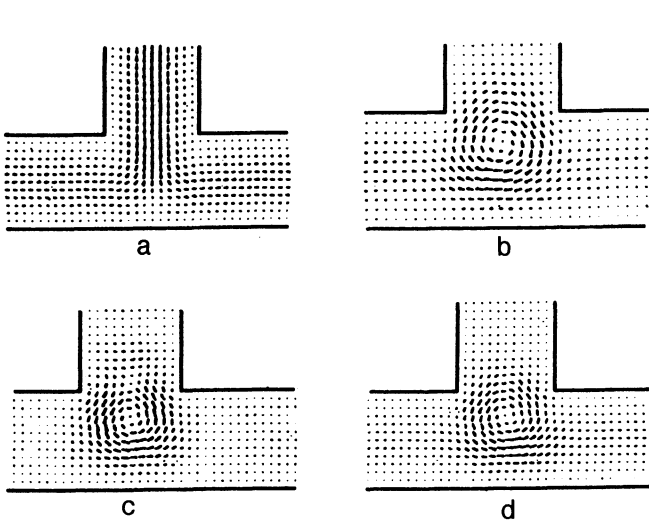


FIG. 5. Current distributions at the input region in the case of single-channel transport for several magnetic fluxes corresponding to the first AB oscillation period: a) $\tilde{\gamma} = 0$; b) $\tilde{\gamma} = 0.25$; c) $\tilde{\gamma} = 0.5$; d) $\tilde{\gamma} = 0.75$ ($d = 12$, $L = 108$, $\epsilon = 20$).

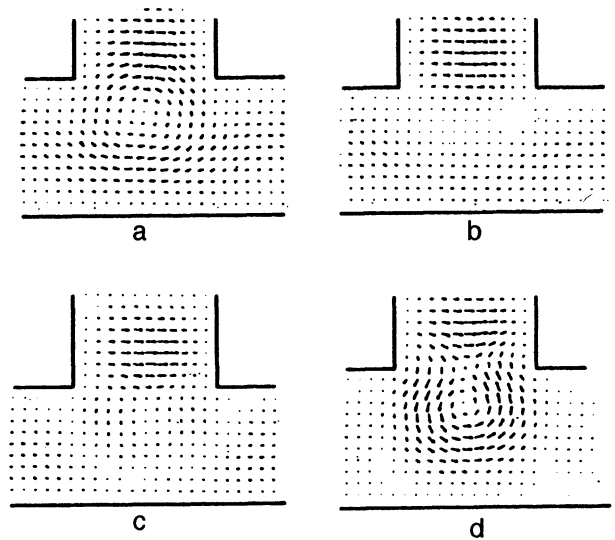


FIG. 6. Current distributions similar to those of Fig. 5 around the second zero in the transmission probability: a) $\tilde{\gamma} = 1.4566$; b) $\tilde{\gamma} = 1.477$; c) $\tilde{\gamma} = 1.4871$; d) $\tilde{\gamma} = 1.5075$.

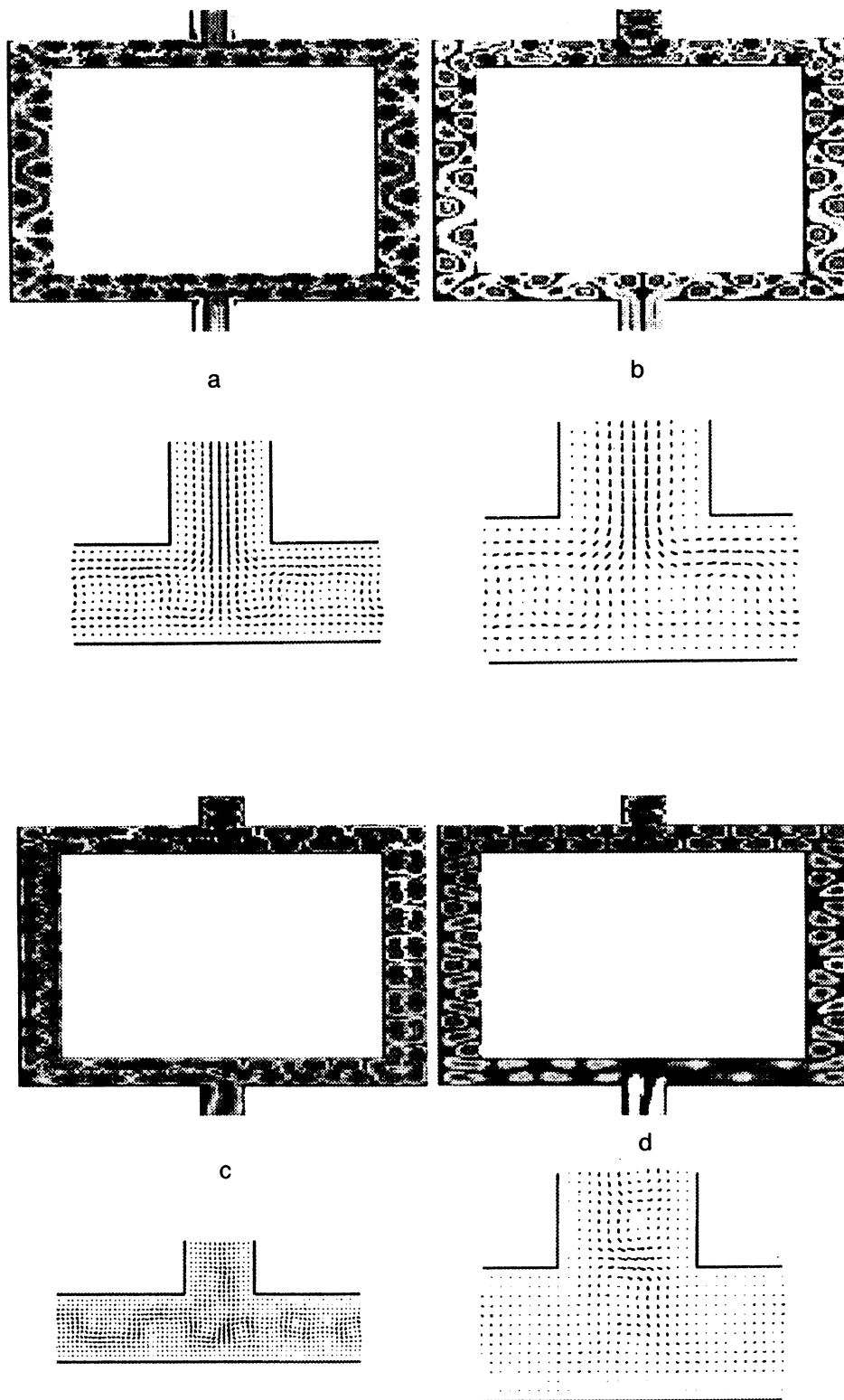


FIG. 7. Contour plots of the wave function $|\psi(x,y)|$ and current distribution at $\epsilon=50$: a) $\tilde{\gamma}=0$; b) $\tilde{\gamma}=0.5$; c) $\tilde{\gamma}=5$; d) $\tilde{\gamma}=5.6$. The current-distribution pattern is shaped as a chain of vortices around the middle line of the loop. The lower plots show only fragments of these chains.

Since vortex states are of primary importance for transport in curved waveguides,^{27,29,35} it is very interesting to calculate the pattern of current density in wide loops:

$$\mathbf{j}(\mathbf{x},\mathbf{y}) = \frac{ie\hbar}{2m} (\psi \nabla \psi^* - \psi^* \nabla \psi) - \frac{e^2}{mc} \mathbf{A} |\psi|^2. \quad (12)$$

The current density was expressed in the numerical calculations using the gauge of Eq. (4) as

$$\frac{j_{mn}}{j_0} = \frac{1}{2} \psi_{m,n} (i \nabla_{mn} - m \gamma) \psi_{m,n}^* - \frac{1}{2} \psi_{m,n}^*$$

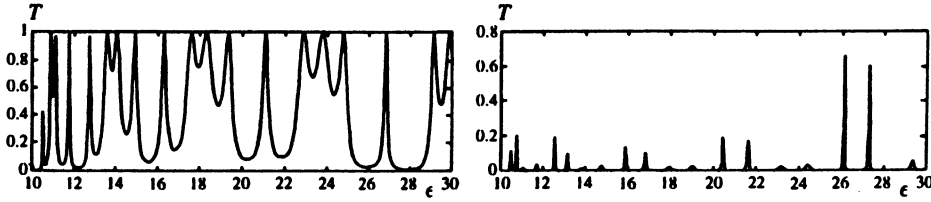


FIG. 8. Transmission probability versus dimensionless energy ϵ [Eq. (9)]: a) $\tilde{\gamma}=0$; b) $\tilde{\gamma}=0.5$. The loop dimensions in mesh widths are $d \times L = 12 \times 108$.

$$\times (i\nabla_{mn} + m\gamma) \psi_{m,n}, \quad (13)$$

where $j_0 = e\hbar/ma_0$, a_0 is the dimension of a unit cell, and

$$\nabla_x \psi_{m,n} = \psi(m+1, n) - \psi(m, n),$$

$$\nabla_y \psi_{m,n} = \psi(m, n+1) - \psi(m, n).$$

In the next section we shall demonstrate that AB oscillations in loops with the finite aspect ratio are followed by very complicated oscillations in the vortex current pattern.

3. NUMERICAL CALCULATIONS

Let us first consider numerical results for narrow loops ($L \gg d$). The width d of bends in the loop equals twelve mesh widths of the grid on which the difference Eq. (11) was solved, the outside loop dimension L equals 108 mesh widths, and the width of the terminal was taken to be d . Figure 2a shows AB oscillations of the probability of transmission across the loop at an energy $\epsilon = 20$. At zero magnetic field only the fundamental mode with $f=1$ is fed into the waveguide. In dimensional units, this energy means that both the metal-terminal and loop widths calculated by Eq. (6) are 10^{-7} cm and the loop dimension is 10^{-6} cm if the Fermi energy is about 1 eV. In GaAs structures, where the Fermi energy is several tens of millielectronvolts and the electron effective mass is $m_* \approx 10^{-28}$ g,⁴² the width is $d \sim 10^{-6}$ cm at a dimensionless energy of 20. In order to identify the AB oscillation period, let us introduce the dimensionless magnetic flux, which is the flux enclosed by the loop opening, $\Phi_{\square} = H_0(L-d)^2$, divided by the flux quantum Φ_0 :

$$\tilde{\gamma} = \frac{\Phi_{\square}}{\Phi_0} = \frac{\gamma(L-d)^2}{d^2}, \quad (14)$$

where the flux γ is defined by Eq. (6). In the limit $d \rightarrow 0$ the AB-oscillation period tends to unity.

Figure 2a demonstrates that in the case of single-channel transport the transmission probability in the range $0 \lesssim \tilde{\gamma} \lesssim 6$ oscillates with a period $\tilde{\gamma} \approx 1$. In terms of magnetic length, this range is $1.3d \gtrsim l_H \gtrsim \infty$. In the next range of magnetic flux, $6 \lesssim \tilde{\gamma} \lesssim 10$, AB oscillations are irregular and quantum fluctuations are important. The importance of quantum fluctuations in this range can be seen from the relationship

$1.3d \lesssim l_H \lesssim d$. A direct evidence of this effect, however, is shown in Fig. 3, where configurations of $|\psi(x, y)|$ for different enclosed fluxes are given. The graph shows four configurations corresponding to maxima and minima of the transmission probability indicated by arrows in Fig. 2a. For comparison Fig. 4 shows four configurations of $|\psi(x, y)|$ on one period of AB oscillations at low magnetic fields. One can see that in the region of irregular oscillations the pattern is blurred over the whole bend in the loop, whereas in the region of regular oscillations the pattern is clearly periodic over the entire conducting path and is gradually deformed by the magnetic flux.

The distinctive feature of AB oscillations in the electron transport in the single-channel case is that the transmission probability is exactly zero at points $\tilde{\gamma} \approx m + 1/2$. If electron currents are assumed to be laminar in the loop segments, the inside and outside trajectories enclose different magnetic fluxes.¹⁸ The conditions that the phase difference between electrons passing along the left and right paths equals π for all possible trajectories cannot be fulfilled, and it seems that the transmission probability cannot vanish. The numerical calculation of the current distribution for different magnetic fluxes in the range of regular oscillations indicates that in reality the electron transport is laminar throughout the structure only at zero magnetic field, so that phases of electrons conducted via the right and left path are equal and the transmission probability is a maximum. But as soon as the magnetic flux is nonzero, a vortex state is formed at the input region (Fig. 5b) and the states in the right and left branches are mixed. Therefore it is impossible to specify the flux enclosed by a particular trajectory.

Near the points $\tilde{\gamma} = m + 1/2$ a vortex-antivortex pair is formed at the input junction, so the phase shifts due to the magnetic flux along inside and outside trajectories in the loop are equalized and the transmission probability goes to zero (Fig. 5c). At this moment the state is degenerate with respect to current reversal, and the sign of vortex chirality is inverted. Figure 6 shows current patterns around the second zero of the AB oscillations at an input electron energy $\epsilon = 20$. This graph indicates that even a small change in the magnetic flux leads to a radical restructuring of the current

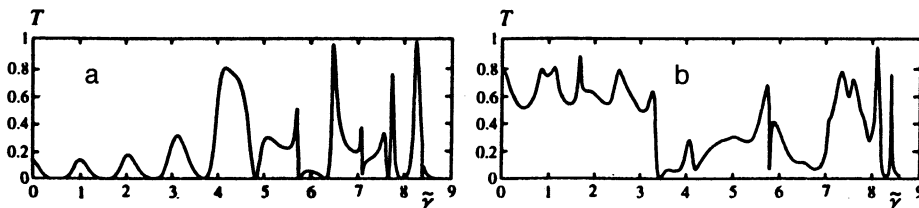


FIG. 9. AB oscillations of transmission probability in the loop with $L/d=7$: a) $\epsilon=20$; b) $\epsilon=50$.

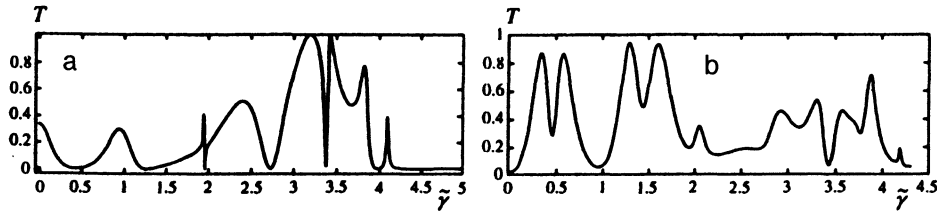


FIG. 10. AB oscillations of the transmission probability in the loops with $L/d=4$: a) $\epsilon=20$; b) $\epsilon=50$.

pattern. The reversal of the chirality of vortex states at an energy corresponding to zero conductance was also reported in Ref. 29, where a curved waveguide with two bends was discussed. On the second half-period of AB oscillations the current pattern is similar to that of the first half-period, except that the current direction is reversed. Figure 5(d) shows the current pattern at a magnetic flux corresponding to 3/4 of the oscillation period, and it is nearly identical to that in Fig. 5b, but with reversed current directions. If we renormalize the magnetic length taking into account the real period of the oscillations, the region of regular oscillations is described in practically all cases by the relationship $l_H \gtrsim 1.3d$, where

$$l_H = \sqrt{\frac{1}{2\pi\tilde{\gamma}}}(L-d).$$

Figure 2b shows AB oscillations of the transmission probability at an energy $\epsilon=50$ at which, according to Eq. (9), the second waveguide mode ($f=2$) is involved (two-channel transport). Besides, an electron can switch between these two modes in this case.^{27,29,36,43} The curve of oscillations demonstrates that this modification leads to radical changes, and oscillations are irregular after two regular periods starting with $\tilde{\gamma} \gtrsim 2.5$. In the two-channel mode two electron half-waves can be inserted between path boundaries. As a result, the effective magnetic length is shorter, and the condition of electron transport without fluctuations becomes $l_H \gtrsim 1.8d$. The range of regular AB oscillations is reduced accordingly, as seen in Fig. 2b. But the pattern of the current distribution is different from the single-channel case, and even at zero magnetic field the electron transport in the loop is vortex-like, so the current distribution pattern is a chain of

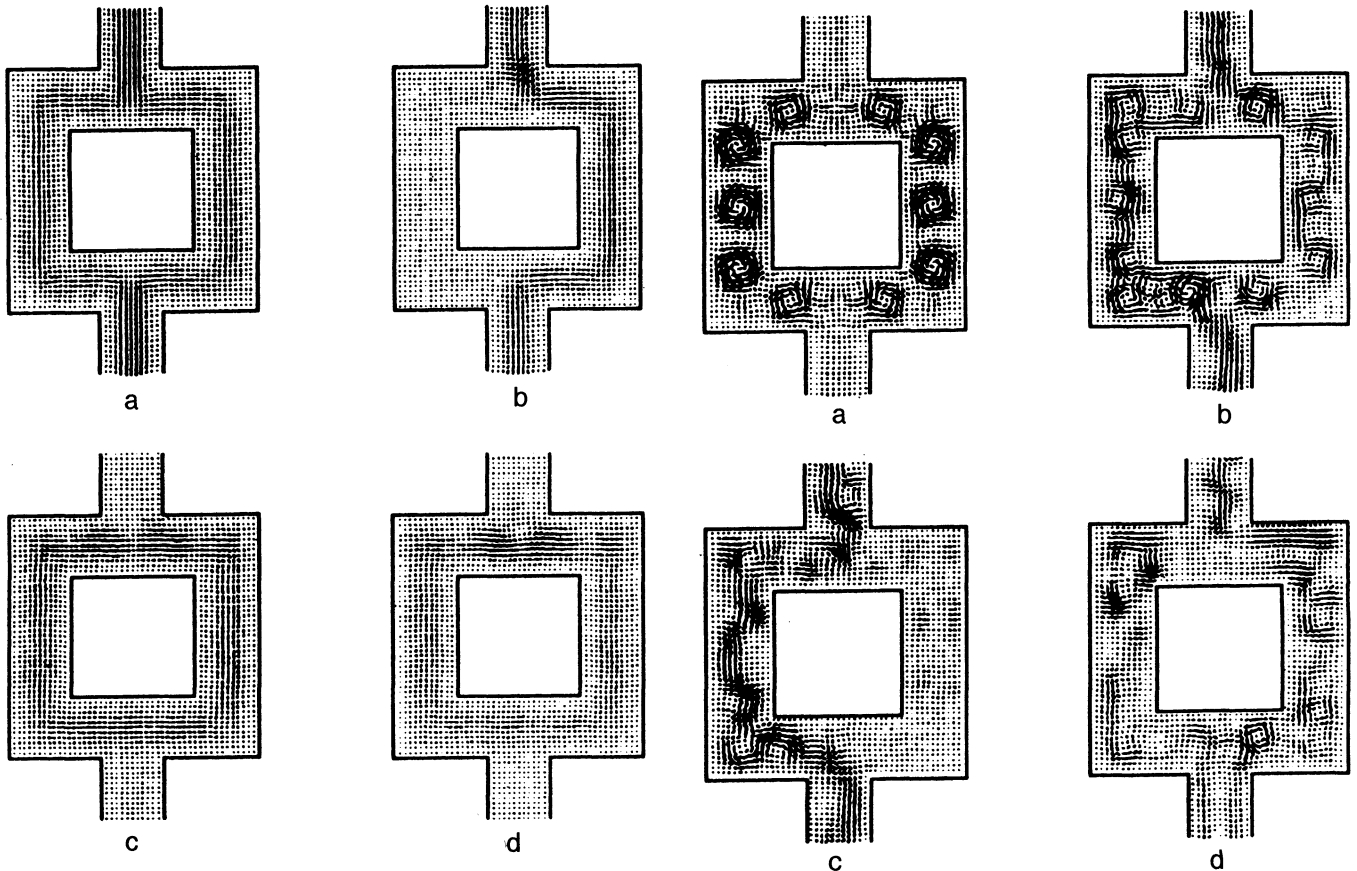


FIG. 11. Current distributions in the loop with a finite aspect ratio ($L/d=4$) in the case of single-channel transport for $\epsilon=20$: (a) $\tilde{\gamma}=0$; (b) $\tilde{\gamma}=1$; (c) $\tilde{\gamma}=1.966$; (d) $\tilde{\gamma}=1.9695$. Graphs c and d correspond to anomalies in AB oscillations around $\tilde{\gamma}=2$ shown in Fig. 10 for $\epsilon=20$.

FIG. 12. Current distributions in a loop with a finite aspect ratio ($L/d=4$) in the case of two-channel transport for $\epsilon=50$: (a) $\tilde{\gamma}=0$; (b) $\tilde{\gamma}=0.3724$; (c) $\tilde{\gamma}=3.0$; (d) $\tilde{\gamma}=3.8675$.

vortices, part of which is shown in Fig. 7. As a consequence, the conductance as a function of the magnetic flux does not vanish, except in the range $l_H \lesssim d$, where the wave function is totally localized at the input junction. In the case of the three-channel transport, there are two vortex chains, etc. This effect was also reported in Ref. 29, where the scale of the vortex pattern changed abruptly at certain energies of electrons launched into a waveguide with two bends. These critical energies correspond to the change in the number of transport channels in the waveguide.

To end our discussion of AB oscillations in the loop transmission at low electron energies and a small aspect ratio, note that amplitudes of regular oscillations are notably smaller than in the case of higher energies. The cause of this is the square shape of the loop, whose corners generate bound states of a transport electron.^{44,45} As a result, an electron propagates across an effective potential relief with two potential wells in one bend of the loop. The transmission probability plotted against the electron energy at a fixed magnetic flux in fact demonstrates a typical resonant tunneling nature (Fig. 8).

Now we shall discuss calculations for loops with larger d/L ratios. Figures 9 and 10 show AB oscillations in loops with dimensions $d \times L = 12 \times 84$ ($d/L = 1/7$) and 12×48 ($d/L = 1/4$) in terms of the mesh width. As we might expect, AB oscillations become aperiodic at smaller magnetic fluxes. The range of periodic AB oscillations, like in the case of a narrow loop, is approximately described by the inequality $0 \lesssim \tilde{\gamma} \lesssim 2$ or $l_H \gtrsim 2d$. The range of irregular oscillations can be described as $2 \lesssim \tilde{\gamma} \lesssim 4$ or $d \gtrsim l_H \gtrsim 2d$. Figure 11 shows patterns of the current distribution for single-channel transport in an wide loop, and Fig. 12 shows the distribution for the two-channel transport. The latter shows that even in zero magnetic field the current pattern consists of a vortex chain. At a finite magnetic field this pattern becomes more complicated, and at a large magnetic flux, corresponding to irregular AB oscillations, the current pattern contains a complex set of vortex and antivortex states.

Summarizing the computer simulations discussed above, we come to the following conclusions. The patterns of the current distribution and wave function of an electron propagating across a mesoscopic loop at small electron energies and magnetic fluxes help us to discover fine mechanisms which control single current vortices in the range of regular AB oscillations. At a high magnetic flux in the range of irregular oscillations, our calculations demonstrate the importance of quantum fluctuations, which eventually spread electron wave functions. In the energy range where several channels are involved in the electron transport (which is the case in metal loops), the current pattern convective and consists of one, two, etc., vortex chains. As a result, the electron transport becomes totally irregular. Thus the cause of the AB oscillation irregularity is the vortex structure of the electron current, which consists of a quasiperiodic lattice of vortices acting as Benard cells. As a result, electron trajectories have complex shapes and enclose magnetic flux in a complicated way. Therefore even a small variation in the magnetic field, which brings about small deformation of Benard cells, significantly changes the phase shift on the electron trajectory.

This change equals by the order of magnitude the product of the loop perimeter L and the Benard cell dimension, which is approximately equal to the width d of the bend divided by the number of electron transport channels. An estimate of the number of transport channels in experiments by Webb *et al.*,^{5,17} who studied gold loops with a width $d \approx 40$ nm yields $10^{3/2}$. This means that the current pattern in those loops is quite complex with many vortex chains. In order to study regular AB oscillations, one should take very narrow loops. The widths d of metal loops should be about 1 nm, and that of GaAs structures of the order of 10 nm.

The work was supported by the Russian Fund for Fundamental Research (project No. 94-02-04410), NATO Linkage Grant 93-1602, and by the Krasnoyarsk territory Science Foundation.

¹H. Sakaki, in *Physics of Nanostructures*, ed. by J. H. Davies and A. R. Long (1992), p. 1.

²Y. Aharonov and D. Bohm, *Phys. Rev.* **115**, 485 (1959).

³R. A. Webb, S. Washburn, C. P. Umbach, and R. B. Laibowitz, in *SQUID '85, Superconducting Quantum Interference Devices and their Applications*, ed. by H. D. Hahlbohm and H. Lubbig (Walter de Gruyter, New York, 1985), p. 561.

⁴R. A. Webb, in *Quantum Coherence* (World Sc. Publ., Singapore, 1990).

⁵S. Washburn and R. A. Webb, *Adv. Phys.* **35**, 375 (1986).

⁶*The Quantum Hall Effect*, ed. by R. E. Prange and S. M. Girvin (Springer-Verlag, New York, 1987).

⁷K. von Klitzing, G. Dorda, and M. Pepper, *Phys. Rev. Lett.* **45**, 494 (1980).

⁸B. I. Al'tshuler, A. G. Aronov, and B. Z. Spivak, *Pis'ma Zh. Éksp. Teor. Fiz.* **33**, 101 (1981) [*JETP Lett.* **33**, 91 (1981)].

⁹A. G. Aronov and Yu. V. Sharvin, *Rev. Mod. Phys.* **59**, 765 (1987).

¹⁰Y. Gefen, Y. Ymry, and M. Ya. Azbel, *Phys. Rev. Lett.* **52**, 129 (1984).

¹¹Y. Gefen, Y. Ymry, and M. Ya. Azbel, *Surf. Sci.* **142**, 203 (1984).

¹²M. Buttiker, in *SQUID '85, Superconducting Quantum Interference Devices and their Applications*, ed. by H. D. Hahlbohm and H. Lubbig (Walter de Gruyter, New York, 1985), p. 529.

¹³E. N. Bulgakov and A. F. Sadreev, *Phys. Rev. B* **52**, 11938 (1995).

¹⁴J. P. Carini, K. A. Muttalib, and S. R. Nagel, *Phys. Rev. Lett.* **53**, 102 (1984).

¹⁵D. A. Browne, J. P. Carini, K. A. Muttalib, and S. R. Nagel, *Phys. Rev. B* **30**, 6798 (1984).

¹⁶M. Buttiker, Y. Imry, R. Landauer, and S. Pinhas, *Phys. Rev. B* **31**, 6207 (1985).

¹⁷R. A. Webb, S. Washburn, C. P. Umbach, and R. B. Laibowitz, *Phys. Rev. Lett.* **54**, 2696 (1985).

¹⁸A. D. Stone, *Phys. Rev. Lett.* **54**, 2692 (1985).

¹⁹J. K. Jain and S. A. Kivelson, *Phys. Rev. Lett.* **60**, 1542 (1988).

²⁰J. K. Jain and S. A. Kivelson, *Phys. Rev. B* **37**, 4111 (1988).

²¹B. Shapiro, *J. Phys. C* **19**, 4709 (1986).

²²A. M. Chang, G. Timp, T. Y. Chang, *Sol. St. Commun.* **67**, 769 (1988).

²³S. Bandyopadhyay, S. Chaudhuri, B. Das, and M. Cahay, *Superlattices and Microstructures* **12**, 123 (1992).

²⁴S. Chaudhuri, S. Bandyopadhyay, and M. Cahay, *Superlattices and Microstructures* **11**, 241 (1992).

²⁵S. Chaudhuri, S. Bandyopadhyay, and M. Cahay, *Phys. Rev. B* **47**, 12649 (1993).

²⁶V. M. Ramaglia, F. Ventriglia, and G. P. Zucchelli, *Phys. Rev. B* **48**, 2445 (1993).

²⁷C. S. Lent, *Phys. Rev. B* **43**, 4179 (1991).

²⁸M. Leng and C. S. Lent, *Superlattices and Microstructures* **11**, 351 (1992).

²⁹K.-F. Berggren and Zhen-Li Ji, *Phys. Rev. B* **47**, 6390 (1993).

³⁰R. Landauer, *Phil. Mag.* **21**, 863 (1970).

³¹M. Buttiker, *Phys. Rev. B* **38**, 9375 (1988).

³²C. B. Duke, *Tunneling in Solids* (Academic Press, New York, 1969).

³³E. E. Mendez, in *Physics and Applications of Quantum Wells and Superlattices*, ed. by E. E. Mendez and K. von Klitzing (Plenum Press, New York and London, 1987).

³⁴K. Vacek, A. Okiji, and H. Kasai, *Phys. Rev. B* **47**, 3695 (1993).

³⁵H. Wu, D. W. L. Sprung, and J. Martorel, *Phys. Rev. B* **45**, 11960 (1992).

- ³⁶H. Kasai, K. Mitsutake, and A. Okiji, *J. Phys. Soc. Jap.* **60**, 1679 (1991).
³⁷M. Buttiker, *Phys. Rev. Lett.* **57**, 1761 (1986).
³⁸R. L. Schult, H. W. Wyld, and D. G. Ravenhall, *Phys. Rev. B* **41**, 12760 (1990).
³⁹Y. Avishai and Y. B. Band, *Phys. Rev. Lett.* **62**, 2526 (1989).
⁴⁰Q. Niu and D. J. Thouless, *Phys. Rev. B* **35**, 2188 (1987).
⁴¹S. Datta, *J. Phys. C: Condensed Matter* **2**, 8023 (1987).

- ⁴²L. L. Chang, L. Esaki, and R. Tsu, *Appl. Phys. Lett.* **24**, 593 (1974).
⁴³P. Streda, J. Kucera, and A. H. MacDonald, *Phys. Rev. Lett.* **59**, 1973 (1987).
⁴⁴P. Exner, P. Seba, and P. Stovicek, *Czech. J. Phys. B* **39**, 1181 (1989).
⁴⁵H. Wu and D. W. L. Sprung, *Phys. Rev. B* **47**, 1500 (1993); *Phys. Lett. A* **183**, 413 (1993); *Phys. Rev. A* **49**, 4305 (1994).

Translation provided by the Russian Editorial office.